Available online at www.sciencedirect.com
SCIENCE DIRECT®
Journal of Computational Physics 202 (2005) 298–322
JOURNAL OF COMPUTATIONAL PHYSICS
www.elsevier.com/locate/jcp

A spectral multidomain penalty method model for the simulation of high Reynolds number localized incompressible stratified turbulence

P.J. Diamessis [a,*], J.A. Domaradzki [a], J.S. Hesthaven [b]

[a] *Department of Aerospace and Mechanical Engineering, University of Southern California, University Park, Los Angeles, CA 90089-1191, USA*
[b] *Division of Applied Mathematics, Brown University, Providence, RI 02912, USA*

Received 16 December 2003; received in revised form 7 July 2004; accepted 11 July 2004
Available online 11 September 2004

Abstract

A spectral multidomain penalty method model has been developed for the simulation of high Reynolds number localized stratified turbulence. This is the first time that a penalty method, with a particular focus on subdomain interface treatment, has been used with a multidomain scheme to simulate incompressible flows. The temporal discretization ensures maximum temporal accuracy by combining third order stiffly stable and backward differentiation schemes with a high-order boundary condition for the pressure. In the non-periodic vertical direction, a spectral multidomain discretization is used and its stability for under-resolved simulations at high Reynolds numbers is ensured through use of penalty techniques, spectral filtering and strong adaptive interfacial averaging. The penalty method is implemented in different formulations for both the explicit non-linear term advancement and the implicit treatment of the viscous terms. The multidomain model is validated by comparing results of simulations of the mid-to-late time stratified turbulent wake with non-zero net momentum to the corresponding laboratory data for a towed sphere. The model replicates correctly the characteristic vorticity and internal wave structure of the stratified wake and exhibits robust agreement with experiments in terms of the temporal power laws in the evolution of mean profile characteristic velocity and lengthscales.

Keywords: Spectral multidomain; Penalty methods; Under-resolution; Turbulence; Stratified flow; Wakes

* Corresponding author. Tel.: +1 213 740 9210; fax: +1 213 740 7774.
E-mail addresses: pdiam@spock.usc.edu (P.J. Diamessis), jad@usc.edu (J.A. Domaradzki), jan.hesthaven@brown.edu (J.S. Hesthaven).

0021-9991/$ - see front matter © 2004 Elsevier Inc. All rights reserved.
doi:10.1016/j.jcp.2004.07.007

1. Introduction

1.1. Background: localized stratified turbulence

Stably stratified turbulent flows are ubiquitous in natural fluids [16,33,57]. Due to the restoring effect of buoyancy, any turbulence producing sizable vertical transport and diapycnal mixing occurs locally and episodically at high values of Reynolds number (defined in terms of a characteristic geometric length and a large-scale velocity), $Re \gtrsim O(10^4)$. The stable stratification gives rise to characteristic forms of fluid motion such as internal gravity waves and remarkably organized clusters of quasi two-dimensional horizontal (''pancake'') vortices [17,46,53]. It is of interest to fluid mechanicists, physical oceanographers and meteorologists to not only understand the fundamental physics of stratified turbulence but also correctly parameterize it for use in large-scale circulation models [37]. In this respect, numerical simulations play a critical role. The ultimate objective of a numerical simulation is to provide a *stable* and, *accurate* and *realistic* reproduction of the physics of the geophysical stratified flow under consideration at all relevant spatiotemporal scales and at a tractable computational cost.

The accuracy of a numerical simulation is highly contingent on the choice of numerical discretization. It is well known that spectral discretizations provide the most accurate numerical approximation of the governing equations [4,6,9], particularly in direct numerical simulation (DNS) where one intends to capture the full range of scales of the flow and the only dissipative mechanism at the smallest scales should be molecular viscosity rather than some truncation error-induced artificial damping. Thus, a very accurate description of dissipation and mixing processes may be obtained [50]. Stably stratified homogeneous turbulence is an extremely popular template flow for a stratified turbulent flow, in part due to the ease with which it can be studied by means of DNS [31,36]. Periodic boundary conditions in all three spatial directions may be considered for the simulation of such a flow and thus one may employ straightforward Fourier discretization.

It is questionable, however, how representative space-filling stratified homogeneous turbulence is of its localized geophysical counterpart. Obviously, the accurate reproduction of realistic flow physics also depends on how closely the forcing and boundary conditions of the simulation correspond to those of the original geophysical flow and how well both of the above are accommodated by the discretization scheme. To this end, Fourier discretization is too restrictive. A more flexible discretization scheme is desired which accomodates realistic boundary conditions and is adaptable to the spatial distribution of the external forcing.

An accurate and realistic simulation should also achieve as closely as possible the range of governing parameters associated with the geophysical flows of interest, in particular, their characteristically high values of *Re*. In high *Re* flow simulations, one may be interested in the dynamics of the energy-containing scales of stratified turbulence but may be unable to resolve the smallest, dissipative scales due to restrictions in available computer resources. The introduction of a subgrid scale (SGS) model, providing a reliable coupling between resolved and unresolved scales, is then imperative. The application of a certain class of weakly dissipative SGS models [12] along with high-order numerical methods to *finite domain* under-resolved simulations leads to numerical instabilities detrimental to the long-time integration of the governing equations. Therefore, a discretization scheme is required that not only accommodates more realistic forcing/boundary conditions but also is stable at high *Re* with no adverse impact on the spectral accuracy of the scheme. The two above needs are what motivate not only the remainder of Section 1 but also the development of the spectral multidomain penalty method outlined in this paper.

1.2. Representation/discretization of localized flows

Introducing a non-periodic vertical direction allows for the specification of a more realistic, non-space-filling stratified turbulent flow. In such a case, Fourier cosine/sine discretization may be used in the vertical to maintain spectral accuracy [24,50,61]. Such a scheme however, is restricted to strictly

symmetric Dirichlet/Dirichlet or Neumann/Neumann boundary conditions at the top and bottom of the computational domain. Low-order finite difference schemes overcome this restriction in choice of boundary conditions but degrade the accuracy of the numerical approximation due to their inherent truncation error. A logical first choice is to then use orthogonal polynomial base functions (Chebyshev or Legendre) to discretize the vertical in one single domain, as has been done in the simulation of a stratified shear layer [7]. This approach, however, is associated with a fairly slow computation when any sizable number of vertical grid points ($\gtrsim O(10^2)$) is desired.

Spectral multidomain/spectral element discretizations [9,23] allow one to overcome many of the limitations discussed above. The computational domain is partitioned in subdomains of varying size and order of polynomial approximation. Subdomains communicate with their neighbors via a simple patching condition [4]. The immediate advantages of such an approach are [28]:

1. Flexibility in local resolution which allows *adequate* treatment of strongly localized solutions/energetic flow regions without overresolving smooth/less-active parts of the flow when the location of these regions is known a priori. ''Adequate'' is meant in the sense of capturing the range of scales that are of physical interest in the specific location.
2. Reduced operation count and impact of round-off error compared to a single domain computation with the same number of grid points.

Differences in the formulations of spectral multidomain and spectral element methods are discussed in various textbooks [4,6].

1.3. Spectral element simulations of high Re flows

Spatially continuous spectral element methods have been applied extensively to DNS of engineering flows in complex geometries [9], which becomes costly when even moderate *Re* are desired. However, as already mentioned, geophysical turbulence tends to be governed by high values of *Re* and the efficient realistic-cost simulation of a high *Re* flow is inherently under-resolved. The concept of under-resolution has two components: physical and numerical. From a physical standpoint, an under-resolved simulation does not capture the full range of scales present in the high *Re* flow of interest. A range of scales, spanning from the viscous cut-off to one or more orders of magnitude above it, is not accounted for and a SGS model is required to couple these unresolved scales to the resolved ones. The numerical implication of under-resolution is that molecular viscosity has a negligible impact on the resolved scales and, when an inherently non-dissipative spectral element (or multidomain) method is used, numerical instabilities may grow undisturbed.

The majority of currently used SGS models are based on dissipative eddy viscosities [48]. Recently, however, an alternative approach to SGS modelling has emerged whose only requirement is that the numerical mesh resolves adequately the peak in the energy spectrum of the flow under consideration. The range of resolved scales is divided into two subranges, the physical scales and the estimated (or filtered) scales. Both scale subranges are solutions of the Navier–Stokes equations. The estimated scales, the highest resolved modes of the solution, are subject to some form of periodic filtering. Variants of this modelling approach in large eddy simulation (LES) of turbulence are the estimation model [12], spectrally vanishing viscosity (SVV) schemes [38,40] and the approximate deconvolution method [55]. To best evaluate the effect of the SGS model, all three approaches rely on weakly or non-dissipative high-order methods. Thus, a common prerequisite is that the underlying numerical scheme (particularly in the case of a finite domain) perform stably at asymptotically high *Re* when the SGS model is turned-off. If such stable performance is guaranteed the SGS model does not have to assume the additional role of a stabilizer. Similar principles, i.e., stable performance in the absence of any parameterizations, apply for eddy-resolving spectral element ocean models [34,35].

Unfortunately, when a spectral element (or multidomain) scheme is employed in a finite domain under-resolved simulation, the stability of the numerical scheme is confronted with significant challenges due to the numerical component of under-resolution. In the spectral element ocean model [34,35], under-resolution-driven instability is overcome in part through spectral filtering, the application of an explicit low-pass filter on the spectral approximation of the numerical solution [42]. However, full numerical stability is only ensured through introduction of enhanced numerical viscosities. When enforcing the no-slip condition at the domain boundaries, the numerical viscosities generate thick and non-physical boundary layers which may spuriously bias the internal high Re dynamics of the flow [5]. In the case of the incompressible Navier–Stokes equations, spectral multidomain techniques have only once been applied to relatively high Re localized stratified turbulence, where 4th/5th order subdomains were used [59]. At the higher $Re \approx O(10^4)$ considered, high resolution ($256^2 \times 512$) and an overlapping subdomain scheme in the energetic core of the flow were adequate in dealing with under-resolution-generated instabilities at the subdomain interfaces. The only other existing application of higher order methods to moderately high Re stratified turbulence have been been explicitly filtered 4th order compact finite difference schemes in a single domain [49]. Unstratified higher Re studies using spectral elements have been performed using either spectral filtering [18,45] or the spectral vanishing viscosity formulation [38,40,62]. Again, the Re considered are relatively moderate (e.g. cylinder wake $Re = 3 \times 10^3$ or channel flow of $Re = 7.5 \times 10^3$). The spectral element method has also been used in conjuction with the dynamic estimation model [1] for the simulation of $Re_\tau < 10^3$ channel flow. The eddy viscosity coefficients of the dynamic SGS model suppress any under-resolution problems by treating the energy flux to the unresolved scales as a dissipative process. The combination of such dissipative models with low-order finite difference schemes in the non-periodic vertical direction is responsible for the stable LES simulation of higher Re of channel flows [21] and wakes [13]. Although the truncation error of these low-order schemes provides additional artificial dissipation and thereby achieves higher Re, it also is detrimental to the accuracy of the results.

Following the above discussion, a spectral multidomain scheme, despite its potential, is not foolproof to numerical instability when applied to a strongly under-resolved simulation of an incompressible high Re flow. The absence of any artificial dissipation in the numerical scheme or SGS model leads to instabilities due to aliasing effects [23] closely linked to under-resolved numerical/viscous physical boundary layers [9]. Specifically, Gibbs oscillations develop, which are most pronounced at the physical boundaries and subdomain interfaces. The oscillations are worse with increasing Re (and thus degree of under-resolution) and generate catastrophically interacting artificial internal waves in a stratified flow.

1.4. Spectral multidomain penalty methods

Spectral filtering [23,42] is least effective at the boundaries or subdomain interfaces. Thus, a methodology is needed to ensure the stability of a spectral multidomain scheme in these regions for a highly under-resolved simulation. In this respect, spectral penalty methods are very effective. Combined with spectral filtering they allow the highest attainable Re. Penalty methods [28–30] recognize that numerical instabilities arise because boundary/patching conditions are explicitly enforced and there is no provision that the equation solved is satisfied arbitrarily close to the boundary/subdomain interface. By collocating a linear combination of the equation and boundary/patching conditions (the latter multiplied by a penalty term) at the corresponding spatial locations, the penalty method produces a smooth numerical solution with near-negligible error at the boundaries and interfaces. Unlike conventional spectral element/multidomain schemes, penalty methods are discontinuous at the subdomain interfaces. Spectral multidomain penalty methods (hereafter referred to as SMPM) using moderate spectral filtering, have attained a Re value as high as 3×10^5 [14]. Penalty methods have been used successfully in the multidomain simulation of turbulent reacting flows [14,28] and, in a geophysical context, in a nodal

discontinuous Galerkin formulation of the shallow water equations [22]. However, all the above studies deal with hyperbolic partial differential equations. Only simple, time-independent, one-dimensional elliptical problems were considered in the early work of Funaro [19,20]. The only work which has implemented penalty methods in the simulation of incompressible Navier–Stokes equations (specifically in the velocity–vorticity formulation) [58] utilizes the spatially continuous spectral element discretization, employs penalty terms only at the physical boundaries and is restricted to a fairly low $Re = 10^3$.

1.5. A new application of SMPM to high Re turbulent flows

This paper outlines the main components of a spectral multidomain penalty method developed for the purpose of a stable and spectrally accurate simulations of high Re localized stratified turbulence with a non-periodic vertical direction. This is the first time multidomain penalty methods have been applied to the simulation of incompressible flows, with a particular focus on subdomain interfaces. In the numerical method, the penalty technique is combined with moderate spectral filtering, adaptive subdomain interfacial averaging and a high-order temporal discretization [39]. Since SGS modelling is outside the scope of this paper, it is emphasized that no specific SGS model is used beyond explicit filtering (which may tentatively be viewed as a surrogate to an SGS model, as indicated in Section 5). The stratified turbulent wake of a towed sphere is used as base flow for model validation. The SMPM solver replicates extremely well the laboratory wake dynamics both in terms of quantitative timeseries of mean flow quantities as well as qualitative features of the vorticity field. The transition points between different regimes in the evolution of a stratified wake [51,53] are reproduced correctly.

The basic incompressible stratified flow model, base flow and initialization procedure are discussed in Section 2. The numerical method is presented in detail in Section 3. Results validating the spectral multidomain method are shown in Section 4. A summary is given in Section 5.

2. Incompressible stratified flow model

2.1. Governing equations

This study considers incompressible stratified flow governed by the Navier–Stokes equations under the Boussinesq approximation [41,61]:

$$\frac{\partial \mathbf{u}}{\partial t} = \underbrace{-\frac{1}{2}[\mathbf{u}\cdot\nabla\mathbf{u} + \nabla(\mathbf{u}\cdot\mathbf{u})] + \mathbf{F}_g}_{\mathbf{N}(\mathbf{u})} - \frac{1}{\rho_0}\nabla p' + \nu\underbrace{\nabla^2\mathbf{u}}_{\mathbf{L}(\mathbf{u})}, \tag{1}$$

$$\frac{\partial \rho'}{\partial t} = -\nabla\cdot(\mathbf{u}(\rho' + \overline{\rho}(z))) + \kappa\nabla^2\rho', \tag{2}$$

$$\nabla\cdot\mathbf{u} = 0, \tag{3}$$

$$\text{where} \quad \mathbf{F}_g = -g\frac{\rho'}{\rho_0}\hat{\mathbf{k}}. \tag{4}$$

The five unknowns to solve for are the velocity vector $\mathbf{u} = (u,v,w)$, and the pressure and density perturbations p' and ρ', respectively. The non-linear term in the momentum Eq. (1) is written in the skew-symmetric form to minimize aliasing effects in the numerical solution [9]. The perturbations p' and ρ' originate from the decomposition of the corresponding total values into [41]:

$$p = \overline{p}(x,y,z) + p'(x,y,z,t), \tag{5}$$

$$\rho = \rho_0 + \overline{\rho}(z) + \rho'(x,y,z,t). \tag{6}$$

Following the Boussinesq approximation, the reference pressure, $\overline{p}(x,y,z)$ and density, $\rho_0 + \overline{\rho}(z)$ are in hydrostatic balance:

$$\frac{\partial \overline{p}}{\partial z} = -(\rho_0 + \overline{\rho})g. \tag{7}$$

2.2. Boundary conditions

The computational domain is designed to simulate a portion of a laboratory water tank. The top and bottom boundaries of the domain correspond to the top free surface (considered to be free slip) and bottom wall, respectively, of the tank. The lateral domain boundaries are considered periodic and the horizontal boundary conditions are therefore:

$$(u,v,w,p',\rho')(x,y,z,t) = (u,v,w,p',\rho')(x+L_x,y,z,t), \tag{8}$$

$$(u,v,w,p',\rho')(x,y,z,t) = (u,v,w,p',\rho')(x,y+L_y,z,t). \tag{9}$$

The bottom boundary is a solid wall with no slip boundary conditions:

$$u(x,y,0,t) = 0, \quad v(x,y,0,t) = 0, \quad w(x,y,0,t) = 0. \tag{10}$$

The top boundary is a free-slip free-surface:

$$\left.\frac{\partial u}{\partial z}\right|_{(x,y,L_z,t)} = 0, \quad \left.\frac{\partial v}{\partial z}\right|_{(x,y,L_z,t)} = 0, \quad w(x,y,L_z,t) = 0. \tag{11}$$

The density perturbation is subject to a Dirichlet boundary condition at both vertical boundaries

$$\rho'(x,y,0,t) = \rho'(x,y,L_z,t) = 0. \tag{12}$$

The boundary conditions for the pressure are of purely numerical nature and their discussion is thus deferred to Section 3.1.

3. Numerical method

3.1. Temporal discretization

For the temporal discretization of Eqs. (1)–(3), a high-accuracy pressure projection scheme [39] is employed, which has been well tested in the recent spectral method literature (e.g. [1,38]). According to this scheme, if one integrates Eqs. (1)–(3) in time from level t_n to t_{n+1} one obtains the following semi-discrete equations decomposed into three fractional steps for $\mathbf{u}$:

$$\frac{\hat{\mathbf{u}} - \sum_{q=0}^{J_i-1} \alpha_q \mathbf{u}^{n-q}}{\Delta t} = \sum_{q=0}^{J_e-1} \beta_q \mathbf{N}(\mathbf{u}^{n-q}), \tag{13}$$

$$\frac{\hat{\hat{\mathbf{u}}} - \hat{\mathbf{u}}}{\Delta t} = -\nabla \phi^{n+1}, \tag{14}$$

$$\frac{\gamma_0 \mathbf{u}^{n+1} - \hat{\hat{\mathbf{u}}}}{\Delta t} = \nu \mathbf{L}(\mathbf{u}^{n+1}). \tag{15}$$

The splitting procedure for ρ' consists of two steps analogous to Eqs. (13) and (15). In Eqs. (13)–(15), a 3rd order backward differentiation scheme (BDF3 with $J_i = 3$) [9] is used to discretize the temporal derivative and enhance the temporal accuracy of the splitting approach. The viscous operator $\mathbf{L}$ is treated fully implicitly. The weakly dissipative nature of such an approximation is helfpul in stability-sensitive under-resolved problems. The non-linear terms N are advanced in time via a third order stiffly stable scheme (SS3 with $J_e = 3$)[39] allowing for maximum value of a stable timestep. The values of the coefficients α_q, β_q and γ_0 for a BDF3–SS3 scheme may be found in Karniadakis et al. [39].

The quantity ϕ^{n+1}

$$\int_{t_n}^{t_{n+1}} \nabla p' \, \mathrm{d}t = \Delta t \nabla \phi^{n+1} \tag{16}$$

is an intermediate scalar field that ensures that the final velocity $\mathbf{u}^{n+1}$ is incompressible. Note that in Eq. (14), it is assumed $\nabla \cdot \hat{\hat{u}} = 0$ and the Poisson equation is solved for the pressure

$$\nabla^2 \phi^{n+1} = \nabla \cdot \left(\frac{\hat{\mathbf{u}}}{\Delta t} \right). \tag{17}$$

The boundary conditions for $\mathbf{u}$ ((10) and (11)) are enforced in Eq. (15) and an analogous approach is followed for ρ'. However, special care must be taken for the correct choice of intermediate boundary conditions for ϕ in Eq. (17). An intermediate boundary condition that ensures high temporal accuracy for the given scheme is [39]

$$\left. \frac{\partial \phi^{n+1}}{\partial z} \right|_b = \left. \sum_{q=0}^{J_e - 1} \beta_q \mathbf{N}(w^{n-q}) \right|_b - \left. \sum_{q=0}^{J_e - 1} \beta_q [\nu \nabla \times (\nabla \times w)]^{n-q} \right|_b, \tag{18}$$

where $|_b$ denotes $z = 0, L_z$ and the coefficients β_q have the same value as in the SS3 scheme of Eqs. (13)–(15). Guermond and Shen [25] prove that the above splitting scheme (Eqs. (13), (14), (15) and (18)) is equivalent to the rotational form of a velocity-correction projection scheme whose second order variant exhibits $O(\Delta t^2)$ accuracy in both $\mathbf{u}$ and ϕ.

3.2. Spatial discretization

In the periodic horizontal direction, Fourier spectral discretization is used with N_x and N_y Fourier modes in the longitudinal and spanwise direction, respectively. Horizontal derivatives are calculated in a straightforward fashion in Fourier spectral space. In the vertical direction, the computational domain is partitioned into M subdomains of variable height H_k and order of polynomial approximation N_k ($k = 1, \ldots, M$) (Fig. 2). Within each subdomain, Legendre spectral discretization is used and for the specific problem under consideration N_k is fixed and equal to a fixed value N in all subdomains. [1] In each subdomain, any function $f(z)$ may be approximated on the Gauss–Legendre–Lobatto grid as [6]:

$$f(z) = \sum_{j=0}^{N_k - 1} \tilde{f}_j P_j(z), \tag{19}$$

[1] In this manuscript, the symbol N may represent two different quantities, the order of polynomial approximation in a subdomain or the Brunt–Vaisala frequency. In a given section of the manuscript, the quantity N specifically refers to is obvious from the context of the accompanying text.

where $\tilde{f}_j$ is the amplitude of the jth Legendre mode and $P_j(z)$ the jth order Legendre approximating polynomial [6]. Spectral multidomain methods are designed as collocation methods [6] and in this study $f(z)$ is approximated in nodal, not modal, form [4,23]:

$$f(z) = \sum_{j=0}^{N_k-1} f(z_j) l_j(z), \tag{20}$$

where $l_j(z)$ is the jth order Lagrange interpolating polynomial (cardinal function) [4,6]. The discrete vertical derivative of $f(z)$ is computed by linearly mapping the global vertical coordinate z within a specific subdomain onto a local coordinate $\zeta \in [-1,1]$ with $\zeta = -1$ and 1 corresponding to the bottom and top end-point of the subdomain, respectively

$$\frac{\mathrm{d}f}{\mathrm{d}z}(z_i) = \frac{\mathrm{d}}{\mathrm{d}\zeta}\frac{\mathrm{d}\zeta}{\mathrm{d}z} f(z_i) = \frac{2}{H_k} \sum_{j=0}^{N_k-1} f(z_j) D_{ij}, \tag{21}$$

where D_{ij} is the Legendre spectral differentiation matrix. Conventionally, D_{ij} is computed as a function of P_j [6]. However, such a calculation is error-prone especially for higher order derivatives, under-resolved functions and high values of N_k [15]. Such errors may prove to be catastrophic in the family of splitting schemes that do not require boundary conditions for the pressure [11] due to the explicit evaluation of third-order vertical derivatives. In the splitting scheme described in Section 3.1, as a safeguard against errors induced by spectral differentiation an alternative vertical derivative calculation technique, described by Costa and Don [8], is used. The above technique and the classical pseudospectral approach [6] are used to compute all the derivatives in the estimation of the non-linear term of Eq. (13).

In any case, as discussed in Section 1.3, at high Re, the existing splitting scheme and spectral multidomain discretization are prone to significant numerical instabilities most evident at the boundaries and subdomain interfaces. The source of these instabilities are aliasing effects driven by thin numerical/physical boundary layers. The instabilities generate spurious energy with increasingly higher and higher frequency content which has a catastrophic effect on the long-term integration of the governing equations [23]. It is imperative to apply stabilization methodologies, namely penalty methods and in addition, spectral filtering and strong adaptive interfacial averaging.

3.3. Spectral multidomain penalty methods

The recent thrust in development of penalty methods originated from the need to implement appropriate boundary conditions for single domain wave-dominated dissipative problems in a manner that is easy, stable and accurate [30]. The direct enforcement of the boundary conditions does not guarantee that the equation is satisfied arbitrarily close to the boundary. At high Re, thin boundary layers and consequently, unresolved gradients develop which contaminate the flow with Gibbs oscillations through aliasing. As already discussed in Section 1.4, spectral filtering does damp these oscillations in the domain/subdomain interior but is least effective near the boundaries/interfaces. When using a collocation method as is often done with Legendre/Chebyshev schemes, this problematic behavior may be overcome by collocating both the equation and the boundary condition at the physical boundary, the latter multiplied by a penalty coefficient. As a result, the eigenvalues of the associated differential operators are modified [30] and a smooth numerical solution is obtained subject to an error (penalty) equal to the order of the spectral scheme. The spectral accuracy of the numerical scheme is negligibly impacted and one may compute stably the high Re internal dynamics of the flow without having to resolve the thin numerical/viscous physical boundary layers. Consequently, penalty methods are a key enabling technique for the simulation of localized high Re turbulence.

In the case of spectral multidomain discretization, the core of the penalty method is similar to that of the single domain case [28]. Each individual subdomain may be treated as a single domain whose interfaces support patching conditions that act as open boundary conditions through which information is exchanged with adjacent subdomains. The exact nature of the patching conditions depends on whether the equation is parabolic or hyperbolic. In both cases, the patching conditions are such that C_0 and C_1 continuity is enforced only weakly since the interface of two adjacent subdomains corresponds to the same location in physical space but to two separate grid-points. Thus, the penalty method is inherently discontinuous and it is this weak continuity on the numerical grid that allows for a more stable and smooth numerical solution at the subdomain interfaces.

In terms of the splitting scheme outlined in Section 3.1, the penalty method is applied at two different levels in the incompressible Navier–Stokes equations. The explicit non-linear term advancement is treated as a hyperbolic equation whereas the implicit viscous term treatment as a parabolic equation (in this section all subsequent equations are written as a function of the u-velocity without loss of generality):

$$\frac{\partial u}{\partial t} = \mathbf{N}(u), \tag{22}$$

$$\frac{\partial u}{\partial t} = \nu \mathbf{L}(u). \tag{23}$$

The temporal derivatives in Eqs. (22) and (23) are only approximations to those appearing in Eqs. (13)–(15).

Consider first Eq. (22). Here Gibbs oscillations at subdomain interfaces must be suppressed. The boundary conditions, imposed strictly in Eq. (15), are not incorporated in the penalty treatment of the hyperbolic problem. Well-posedness dictates that in each subdomain of index-k and uniform order $N_k = N$ (all subsequent penalty formulations are valid for variable N_k as well), Eq. (22) be subject to the following set of patching conditions at the bottom and top subdomain interfaces, respectively:

$$\begin{aligned} &\alpha u_0^k = g_1^k(t), \quad \text{where } g_1^k(t) = \alpha u_N^{k-1}, \\ &\gamma u_N^k = g_2^k(t), \quad \text{where } g_2^k(t) = \gamma u_0^{k+1}. \end{aligned} \tag{24}$$

The penalty formulation of (22), in *physical space*, is

$$\frac{\partial u^k}{\partial t} = \mathbf{N}(u^k) - \tau_1^k Q_k^-(z_i^k)\left[\alpha u_0^k - g_1^k(t)\right] - \tau_2^k Q_k^+(z_i^k)\left[\gamma u_N^k - g_2^k(t)\right], \tag{25}$$

where

$$Q_k^-(z_i^k) = \delta_{i0}, \quad Q_k^+(z_i^k) = \delta_{iN}, \tag{26}$$

here δ_{ij} is the Kronecker delta function with subscript i corresponding to the collocation point z_i^k. Following the treatment by Hesthaven of patching conditions as localized open boundary conditions (locally, each interface experiences inflow or outflow), the values of the coefficients α, γ, τ_1^k and τ_2^k are determined by considering the value of the vertical interfacial velocities W_0^k and W_N^k at the previous timesteps. In the discretized form of the equations (where ζ – see Section 3.2 – is the vertical coordinate), if $\hat{n}$ is the vector normal to the subdomain interface, the following cases are distinguished:

$$\begin{cases} W_0^k \cdot \hat{n}_0 \geqslant 0: & \alpha = 0, & \tau_1^k = 0, \\ W_0^k \cdot \hat{n}_0 < 0: & \alpha = W_0, & \tau_1^k = \frac{1}{2\omega}\frac{2}{H_k}, \\ W_N^k \cdot \hat{n}_N \geqslant 0: & \gamma = 0, & \tau_2^k = 0, \\ W_N^k \cdot \hat{n}_N < 0: & \gamma = \mid W_N \mid, & \tau_2^k = \frac{1}{2\omega}\frac{2}{H_k}, \end{cases}$$

where

$$\omega = \frac{2}{N(N+1)} \tag{27}$$

and H_k is the height of the kth subdomain. The values of τ_1^k and τ_2^k are what is used in the discretized formulation of (25). Eqs. (24) and (25) imply weak C_0 continuity at the subdomain interfaces due to the normal advective flux of momentum/mass.

The penalty formulation of (23) is significantly different from that of (22) due to its parabolic nature. Eq. (23) is solved in *Fourier space* and its discretized form for each pair of horizontal wavenumbers (k_x,k_y) is

$$D^2u - \left(k_x^2 + k_y^2 - \frac{\gamma_0}{\nu\Delta t}\right)u = -\frac{\hat{\hat{u}}}{\nu\Delta t}, \tag{28}$$

where

$$D \equiv \frac{\partial}{\partial z}$$

and u is the value of the velocity at timestep $n+1$. It is immediately obvious that in the case of significantly high Re, (28) has excessively thin numerical boundary layers of thickness $O(\sqrt{\nu\Delta t})$ whose resolution requires prohibitively high number of grid points at the boundary to be resolved [4,9]. As a result, a singularly perturbed boundary value problem arises which has serious repercussions on the stability of the numerical solution. In addition, at high Re, strict enforcement of C_0 and C_1 continuity in the solution of (28) overexcites the higher Legendre modes resulting in spurious oscillatory behavior at the subdomain interfaces. For the case of the under-resolved Navier–Stokes equations, the neglect of any penalty terms for the non-linear term computation compounds these oscillations through aliasing effects.

To derive the penalty form of (28) one defines a small quantity

$$\varepsilon \equiv \left(k_x^2 + k_y^2 - \frac{\gamma_0}{\nu\Delta t}\right)^{-1} \tag{29}$$

and recasts (28) as

$$u - \varepsilon D^2 u = \varepsilon\frac{\hat{\hat{u}}}{\nu\Delta t} = F. \tag{30}$$

The boundary operators in each subdomain are determined by well posedness and the elliptical nature of (30) and are given by:

$$\begin{aligned} &\alpha u_0^k - \beta\varepsilon\frac{\partial u_0^k}{\partial z^k} = g_1^k(t), \quad \text{where } g_1^k(t) = \alpha u_N^{k-1} - \beta\varepsilon\frac{\partial u_N^{k-1}}{\partial z^{k-1}}, \\ &\gamma u_N^k + \delta\varepsilon\frac{\partial u_N^k}{\partial z^k} = g_2^k(t), \quad \text{where } g_2^k(t) = \gamma u_0^{k+1} + \delta\varepsilon\frac{\partial u_0^{k+1}}{\partial z^{k+1}}. \end{aligned} \tag{31}$$

Thus, the penalty formulation of (30) is

$$\varepsilon D^2 u - u + F - \tau_1^k Q_k^-(z_i^k)\left[\alpha u_0^k - \beta\varepsilon\frac{\partial u_0^k}{\partial z^k} - g_1^k(t)\right] - \tau_2^k Q_k^+(z_i^k)\left[\gamma u_{N_k}^k + \delta\varepsilon\frac{\partial u_N^k}{\partial z^k} - g_2^k(t)\right] = 0, \tag{32}$$

where $Q_k^-(z_i^k)$ and $Q_k^+(z_i^k)$ are defined in (26). It is obvious that (31) and (32) enforce weak C_0 and C_1 continuity at the subdomain interfaces. At the physical boundaries, $g_1^1(t) = g_1(t)$ and $g_2^M = g_2(t)$, where $g_1(t)$ and $g_2(t)$ are the boundary conditions (10)–(12). In the case of non-homogeneous boundary conditions (as may happen with the pressure, discussed below), $g_1(t)$ and $g_2(t)$ are not the exact physical conditions but a modified form that ensures the correct term balance in (31). The coefficients α, β, γ and δ are set

to 1 at each subdomain interface and at the physical boundaries, their values are set to satisfy the physical boundary conditions. The discretized form of (32) supplemented by (31) results in the solution of a linear system of equations where the coefficient matrix is band-diagonal with bandwidth N and may be solved through a variety of existing fast LU solvers. Finally, the coefficients τ_1^k and τ_2^k for the discrete equations (where ζ is the mapped vertical coordinate) are determined by specific stability constraints, for the following cases [30]:

1. Physical boundary with Dirichlet condition:

$$\tau_1^1 = \frac{\varepsilon}{\alpha\omega^2}\left(\frac{2}{H_0}\right)^2, \quad \tau_2^M = \frac{\varepsilon}{\delta\omega^2}\left(\frac{2}{H_M}\right)^2, \tag{33}$$

   where ω is defined in (27).
2. Physical boundary with Neumann condition:

$$\tau_1^1 = \frac{1}{\beta\omega}\frac{2}{H_0}, \quad \tau_2^M = \frac{1}{\delta\omega}\frac{2}{H_M}. \tag{34}$$

3. Subdomain interface with Robin patching condition:

$$\begin{aligned} \tau_1^k &= \frac{1}{\omega\varepsilon\beta}\left[\varepsilon + 2\kappa_1 - 2\sqrt{\kappa_1^2 + \varepsilon\kappa_1}\right]\frac{2}{H_k}, \\ \tau_2^k &= \frac{1}{\omega\varepsilon\delta}\left[\varepsilon + 2\kappa_2 - 2\sqrt{\kappa_2^2 + \varepsilon\kappa_2}\right]\frac{2}{H_k}, \end{aligned} \tag{35}$$

   where $\kappa_1 = \omega\alpha/\beta$ and $\kappa_2 = \omega\gamma/\delta$. In the numerical implementation of a Neumann boundary condition, the value indicated by (34) should be strictly adhered to. For Dirichlet/Robin conditions, the values indicated in (33) and (35) are the lower bound of associated stability requirements. In the simulations of this paper, the penalty coefficients for a Dirichlet condition are kept fixed at the value prescribed above. However, the upper stability bound on the penalty coefficient of a Robin patching condition is of $O(\varepsilon^{-1})$ or greater than the corresponding lower bound [30]. It was found that using a value equal to that of (35) multiplied by a factor of $O(\sqrt{\varepsilon^{-1}})$ increased the stability of the scheme at the subdomain interfaces. An increased value of an interfacial penalty coefficient corresponds to stronger enforcement of the patching conditions and thereby more local dissipation leading to increased stability.

The penalty treatment of (28) is applied to the Poisson equation for the pressure (17) in spectral space for any given pair of horizontal Fourier wavenumbers (k_x,k_y) because (17) is a one-dimensional Helmholtz equation. The only exception is the (0,0) Fourier mode of ϕ which, however, is irrelevant to the computation because the corresponding mode of $\hat{w}$ is zero due to incompressibility and the boundary conditions for w while the (0,0) modes of $\hat{\hat{u}}$ and $\hat{\hat{v}}$ are not ϕ-dependent.

Note that the use of SMPM discretization allows maximum flexibility in the choice of boundary operators (Dirichlet/Neumann/Robin and homogeneous/non-homogeneous). Thus, the existing spectral multidomain model is amenable to the study of geophysical flows with complex boundary forcings (wind stress/buoyancy flux).

3.4. Spectral filtering

For the grid resolutions considered in this paper, penalty methods allow an increase of the value of *Re* by roughly two orders of magnitude. However, even such an increase is not sufficient to attain values of *Re* typical of laboratory wake experiments and beyond. Some form of a hyperviscous operator is needed to

ensure stability for these high *Re*. In practice, what is used instead, which has the same effect but avoids additional stiffness and subsequent timestep limitations, is the application of a low-pass spectral filter on the numerical solution whose convergence rate is thereby enhanced [23]. As long as certain basic requirements [23,42] are satisfied, no unique choice of a filter function is required and in this study, an exponential filter [23] is used

$$\sigma(k) = \begin{cases} 1, & 0 \leqslant k \leqslant k_c, \\ \exp\left[-\alpha\left(\frac{k-k_c}{N-k_c}\right)^p\right], & k_c \leqslant k \leqslant N, \end{cases} \tag{36}$$

where p is the filter order, k_c the filter lag and $\alpha = -\ln \varepsilon_M$ with ε_M being the machine precision. The filtered solution f^F may now be expressed in terms of the modes of the numerical solution as:

$$f^F(z_i) = \sum_{j=0}^{N_k-1} \sigma(k_j)\tilde{f}_j P_j(z_i). \tag{37}$$

where k_j is the jth discrete Legendre mode. An analogous expression may be written for filtering in Fourier space [23].

A common concern with the implementation of spectral filtering in spatially continuous spectral element methodologies is that filtering does not preserve the patching and boundary conditions and thus specific measures need to be adopted [1,3,42]. Such a concern does not exist when using the inherently discontinuous penalty method because the error induced by the filtering operation is of the same order as the penalty scheme [28], i.e., minimal.

In the incompressible spectral multidomain solver presented in this paper, spectral filtering is applied at three levels when advancing the solution from time level (n) to level ($n + 1$). First, to eliminate aliasing effects, filtering is applied in both Fourier and Legendre space after advancing the non-linear terms in (13). The solution to the Poisson equation (17) is filtered in the vertical direction to smooth out any errors induced at the subdomain interfaces due to the discrete estimate of $\partial w/\partial z$. Finally, the solution of (15) is filtered in the vertical. The order of the Legendre filter is the same in all three levels.

For the *Re* under consideration, use of spectral filtering is the inevitable price when confronted with the associated high-degree of under-resolution. Filtering should not be viewed as a waste of resolution because a significant percentage of modes of the numerical solution (O(40−45%) in Legendre space and O(70−75%) in Fourier space) are not directly affected by the filtering procedure. The filtered modes act as a sink of both numerical noise and energy flux from the large scales. Although their content is not necessarily physically correct, their presence is needed to maintain the stability and spectral accuracy of the solution at the larger resolved (physical) scales.

3.5. Strong adaptive interfacial averaging

Although filtering enhances even further the stability properties of a spectral multidomain penalty scheme, the subdomain interfaces occasionally exhibit a propensity for numerical instability. Within each subdomain, using the transformed coordinate ζ, application of the exponential filter of (36) is equivalent to incorporation in the equation of the differential operator [23]

$$\left[\sqrt{1-\zeta^2}\,\frac{\partial}{\partial\zeta}\right]^p. \tag{38}$$

Obviously, (38) indicates that spectral filtering is least effective near the subdomain interfaces where the highest Legendre modes are inherently most oscillatory [6]. To prevent the development and subsequent growth of any such interfacial singularities a simple adaptive interfacial averaging technique is used. Once

the final value of the numerical solution for (u,v,w,ρ') has been obtained in physical space, at the top interface of the kth subdomain, when the following criterion is met [14]

$$\frac{|\, u_0^{k+1} - u_N^k \,|}{|\, u_0^{k+1} + u_N^k \,|} > C_{\text{ave}}, \tag{39}$$

an averaging operation is performed

$$u_N^k = u_0^{k+1} = \tfrac{1}{2}\left(u_1^{k+1} + u_{N-1}^k\right). \tag{40}$$

The coefficient C_{ave} is set equal to 0.005. Eq. (40) was found to be more effective than the technique used by Don et al. [14]. Including the interfacial points in the averaging and even more so restricting the averaging to the interface was found to not eliminate troublesome spikes in the solution. The averaging essentially adds some weak local artificial dissipation to the scheme and is usually required for only a small fraction (O(0.1%)) of the subdomain interfaces.

4. Results

4.1. Problem geometry

The base flow chosen to validate the spectral multidomain penalty model is a stratified turbulent wake with non-zero net momentum. Such a flow corresponds to the mid-to-late time wake of a sphere of diameter D towed with a velocity U in a linear density stratification of frequency N, where

$$N^2 \equiv -\frac{g}{\rho_0}\frac{\mathrm{d}\overline{\rho}}{\mathrm{d}z}. \tag{41}$$

Note that the spatial discretization does not account for the sphere and focuses only on the flow generated in its wake. The computational domain of dimensions $L_x \times L_y \times L_z$ is shown in Fig. 1 and corresponds to a window fixed in space with respect to the moving sphere, as do the laboratory measurements [54]. Behind the sphere, the wake is considered to be statistically stationary. The periodicity assumption in the x-direction is valid because the length of the computational domain is much smaller than the total wake length [13]. The spanwise periodicity assumption is also valid provided the horizontal lengthscale of the wake does not become excessively large. Due to spanwise periodicity, internal waves radiated by the wake re-enter the computational domain and thus after a certain point later in time, the internal wave field does not correspond to its experimental counterpart. However, by that time the flow is efficiently decomposed into internal waves and quasi-two-dimensional vortical modes and analysis of the latter [46] is possible in isolation.

4.2. Initialization: replacing the sphere

Although the sphere is not accounted for in the computation, its effect must be incorporated in the initial condition. The initial flow field is the superposition of an axisymmetric Gaussian mean velocity profile and a turbulent fluctuation field

$$\mathbf{u}(x,y,z,t) = U_X(y,z,t) + \mathbf{u}'(x,y,z,t). \tag{42}$$

The X subscript indicates averaging in the streamwise direction. The magnitude and distribution of mean and fluctuating velocity fields are specified based on available vertical profile measurements of stratified sphere wakes [51–54] at $Nt = 3$ (downstream distance from the sphere, $x/D = 6$).

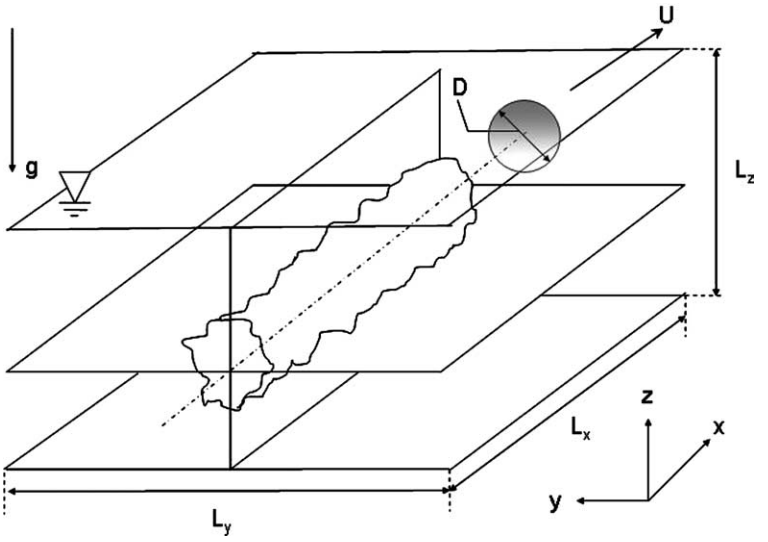

Fig. 1. Computational domain for the simulation of a mid-to-late time momentlumless stratified turbulent wake. The wake was originally generated by a sphere of diameter D, towed with a velocity U, which however is not present in the computational domain. The domain dimensions are $L_x \times L_y \times L_z$. Consistent with the salt-stratified water tank the domain has a solid wall bottom and free-slip top and when needed, a linear stable density stratification may be imposed. Shown are also the horizontal and vertical centerplane where the experimental data used in the initial condition are sampled.

The mean velocity profile is a Gaussian:

$$U_X(y,z,t) = U_0 \exp\left[-\frac{1}{2}\left(\frac{y-\frac{1}{2}L_y}{L_Y}\right)^2 - \frac{1}{2}\left(\frac{z-\frac{1}{2}L_z}{L_Z}\right)^2\right], \tag{43}$$

where U_0 is the maximum centerline velocity and L_Y and L_Z the initial horizontal and vertical lengthscales, respectively. Initially, one sets $V_X = W_X = 0$.

The fluctuating profile is also taken from laboratory data at $Re = 5 \times 10^3$ and $Fr = 4$. The x-averaged r.m.s. (root mean square) distribution of the fluctuating velocity is assumed to be axisymmetric and equipartitioned among its three components

$$u'_X(r,t) = v'_X = w'_X = U_0\left[\alpha_1\left(\beta_1\frac{r^2}{r_p^2}\right)\cdot\exp\left(-0.5\frac{r^2}{r_g^2}\right)\right], \tag{44}$$

where $r = ((y-y_0)^2 + (z-z_0)^2)^{1/2}$. Although the assumptions of axisymmetry and energy equipartition are debatable at $Nt = 3$, horizontal profiles from experiment are available from $Nt = 9$ onwards and a small degree of extrapolation is required in specifying the initial condition in the horizontal direction in the simulations (see Section 4.4). A delayed onset of asymmetry may result but its effect on later wake statistics is negligible. Ideally, one would initialize the model with runs from simulations of stratified flow around a sphere but a spectral multidomain scheme for such a simulation would be a challenge of its own. In addition, low-order scheme-based studies of sphere wakes have been restricted to $Re = 200$ [27].

The three-dimensional fluctuating velocity field is constructed as spectrally random noise in three-dimensional Fourier space with a $k^{-5/3}$ energy spectrum. An inverse Fourier transform is applied to convert the noise into physical space and in the vertical the fields are projected on the non-uniform Gauss–Lobatto–Legendre grid of each subdomain. Finally, the data is windowed in the envelope of the r.m.s. profile of Eq. (44). Use of white noise is avoided because it is unphysical and detrimental to the stability of the numerical solution.

The initial density field is assumed to be an unperturbed linear density stratification. Transients due to the gravity-induced adjustment of the density field to the turbulence [10] have no significant effect on later wake dynamics.

Initially, the fluctuating and mean velocity fields are uncorrelated. Thus, a preliminary "relaxation" simulation [13] is run to generate a physically realistic velocity field. During relaxation, the flow is forced to maintain constant mean and r.m.s. fluctuating velocity profiles according to Eqs. (43) and (44), while the spatial distribution of the turbulent fluctuations, and thus the Reynolds stresses, is allowed to vary.

4.3. Run description

The spectral multidomain penalty method model was used to simulate mid-to-late time stratified turbulent wakes with non-zero net momentum at Reynolds number $Re = UD/\nu = 5 \times 10^3$ and 2×10^4 and internal Froude number, $Fr = U/(DN) = 4$ and ∞. U and D are the tow velocity and diameter of the virtual sphere to which the initial wake condition at $Nt = 3$ would correspond to. Re is modified by changing the value of the molecular viscosity ν. $Re = 5 \times 10^3$ and $Fr = 4$ are typical values of laboratory experiments performed by Spedding et al. [51–54]. The choice of Re and Fr values for the simulations was made to illustrate the effect of the turbulent scale separation (increasing with Re) and buoyancy on the dynamics of a turbulent wake. $Re = 2 \times 10^4$ is a maximum Re for the resolution employed in this study, above which under-resolution effects affect the robustness of the simulation.

The computational domain has a horizontal dimension of $L_x \times L_y = 16D \times 16D$ and corresponds to a virtual stratified water tank of height $H = 12D$. Such domain dimensions ensure that the domain exhibits adequate length, width and height to allow for multiple streamwise wavelengths of a vortex shedding instability and also minimize effects of confinement and interaction with the wake's periodic image. A uniform spatial grid is used in the horizontal direction whereas in the vertical the spectral multidomain discretization of Fig. 2 is employed with $M = 5$ non-uniform height subdomains of fixed order of approximation $N_k = N$. The positioning of the subdomains is dictated by the requirement of adequate resolution of the energetic scales of the turbulence in the active regions of the flow, which are known a priori. Increased resolution is available at the energetic core of the wake whereas less is utilized in the less active, internal-wave dominated ambient. The non-uniform Gauss–Lobatto–Legendre grid of the topmost subdomain allows for enhanced resolution of the subsurface region. The ratio of adjacent subdomain heights H_k/H_{k-1} is not

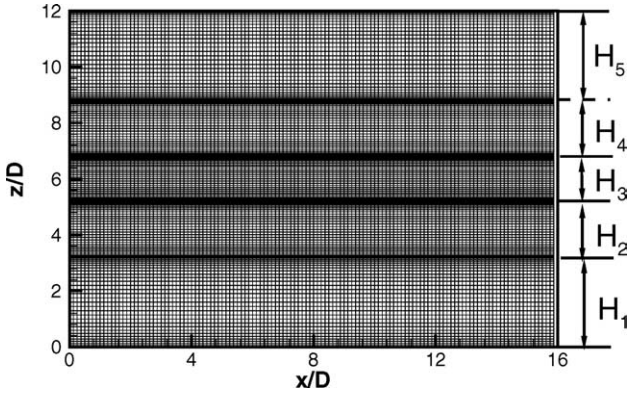

Fig. 2. Oxz section of the numerical grid employed in this study. The horizontal direction employs a spectral Fourier discretization and uniform grid. In the vertical a Legendre spectral multidomain discretization is used with $M = 5$ subdomains of order of approximation N and a local Gauss–Lobatto–Legendre grid. Shown is the vertical grid point distribution for $Re = 5 \times 10^3$ where $N = 32$. $Re = 2 \times 10^4$ employs $N = 48$. The dashed horizontal lines on the right of the figure indicate the position of the subdomain interfaces. Subdomain origins are at $z/D = 0$, 3.2, 5.2, 6.8 and 8.8.

determined analytically and is only restricted by the requirement that it be maintained within the interval [0.5,2]. Otherwise, reflections are observed at the interfaces.

The resolution used for the $Re = 5 \times 10^3$ and $Re = 2 \times 10^4$ runs is $128 \times 128 \times 165$ and $128 \times 128 \times 245$, respectively. The low Re Fourier and Legendre spectral filters are $(p_F,p_L) = (20,8)$ and at the high Re, $(p_F,p_L) = (16,6)$ is used. The filter lag is $k_c = 0$. In the higher Re run, increased under-resolution is countered by increasing N, while keeping H_k fixed (p-refinement), and reducing filter order. The adequacy of resolution for the $Re = 5 \times 10^3$ and 2×10^4 is evident in Fig. 3 which shows one-dimensional spectra of the turbulent kinetic energy (calculated strictly within the wake region) at three different times for the $Fr = \infty$ simulations. For the non-filtered range of scales, the form of all spectra in Fig. 3 is consistent with those observed in the DNS of Gourlay et al. [24] and mixed model LES of Dommermuth et al. [13]. Despite very similar initial spectra at $t = 0s$ (a possible effect of the relaxation procedure), $Re = 2 \times 10^4$ develops different features, primarily the presence of a more extended inertial range of nearly a decade in span. The effect of viscosity on the resolved scales of $Re = 5 \times 10^3$ is evident due to the more rapid drop-off of the spectrum within the range of scales directly unaffected by the filter. In general, the energy spectra drop off smoothly at the smallest scales least affected by the filter. No sign of artificial energy accumulation, an unwanted feature of under-resolution, is observed [4], over the range of scales directly affected by the filter. Instead, the filter produces artificial energy "anti-accumulation" as manifested by the sharp spectral slope in these regions. As discussed in the end of Section 3.4, this sharp drop-off should not be a cause for concern because the higher modes of the numerical solution are not necessarily physically correct.

The computational timestep Δt was chosen as such that the CFL stability criterion be obeyed in all three spatial directions for a 3rd order stiffly stable scheme. The following requirements are imposed:

$$\Delta t \frac{u_{\max}}{\Delta x} < 0.15, \quad \Delta t \frac{v_{\max}}{\Delta y} < 0.15, \quad \Delta t \left[\frac{w}{\Delta z}\right]_{\max} < 0.6. \tag{45}$$

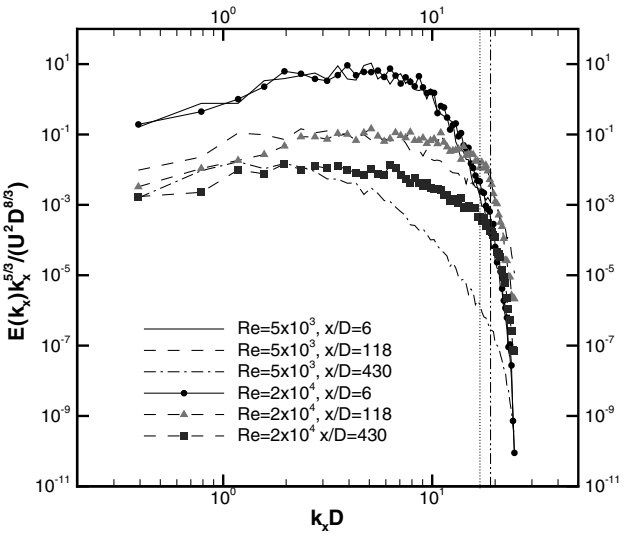

Fig. 3. Normalized one-dimensional spectra of turbulent kinetic energy calculated for $Re = 5 \times 10^3$ and 2×10^4. The streamwise spectra are averages of estimates taken at spanwise locations located in the interval $(y_0 - 2L_Y, y_0 + 2L_Y)$ on the horizontal centerplane. Spectra are shown at initialization of the actual run as well as intermediate and late times. Vertical lines represent the approximate limit over which the filter significantly affects the numerical solution (dash-double dot line: $Re = 5 \times 10^4$, dotted line $Re = 2 \times 10^4$).

In all runs, at $t = 0$, $\Delta t/(D/U) = 0.04$ is used. At later times of a simulation, when the CFL constraint is relaxed, the run may be restarted with a higher timestep. It is imperative that 3rd (not lower) order BDF be used in the restart scheme. In the temporally under-resolved simulations of interest, lower order BDF approximation of the temporal derivative produces excessive artificial dissipation and non-physical decrease of the kinetic energy of the flow. During the first two timesteps of the restart, variable timestep BDF3 [26] and 3rd order Adams–Bashforth schemes [49] are used.

4.4. Setting the initial wake lengthscales and velocities

The initial values of the coefficients in the mean and fluctuating velocity profile Eqs. (43) and (44) are either taken directly or extrapolated from the data of Spedding [51–53]. Given Spedding's observation that the horizontal growth rate of a stratified wake is equal to that of its unstratified counterpart, one may use later time data for $Fr = 4$ and at $x/D = 6$ set $L_Y/D = 0.4$. The initial time $Nt = 3$ falls within the non-equilibrium (NEQ) regime during which U_0 follows a $t^{-0.25}$ power law. Thus, one can estimate from Spedding's data available at $Nt = 5$, a value of $U_0/U = 0.1479$ at $Nt = 3$. Using laboratory data at $Nt = 5$ and the assumption that the constant value of L_Z during the NEQ regime extends as far back as $Nt = 2$, as observed in the self-propelled body experiments of Lin and Pao [43], one estimates $L_Z = 0.4 = L_Y$ at $Nt = 3$. Axisymmetry in mean wake geometry is plausible during the earlier phases of the buoyancy-influenced NEQ regime. In addition, it motivates the choice of an axisymmetric fluctuating velocity profile in Section 4.2. Laboratory data from vertical slices indicate that at $t = 0$ in (44), $\alpha_1 = 0.03375$, $\beta_1 = 1/15$, $r_g/D = 0.35$ and $r_p/D = 0.1$. The $Fr = \infty$ simulations utilize the same initial condition. It is questionable whether two towed body wakes at $Fr = 4$ and $Fr = \infty$ at identical Re and Pr have the same characteristic lengths and velocities at $x/D = 6$. However, the focus of this paper is the reproduction of the stratified wake experimental data and the sole concern with the $Fr = \infty$ wakes is that they obey the appropriate temporal power laws.

All simulations are run until the dimensions of the characteristic vortical structures (see Section 4.5) become large in comparison to those of the computational domain. The spanwise dimension of the domain is most restrictive in the $Fr = 4$ runs, whereas the $Fr = \infty$ simulations experience confinement primarily due to the height of the domain.

4.5. Model validation: qualitative results

Fig. 4 shows isosurfaces of the vertical vorticity ω_z for the $Fr = 4$ simulations at time $Nt = 56$ ($x/D = 112$). The formation of large horizontal (''pancake'') eddies, three-dimensional structures with a large aspect ratio, typical of the late evolution of stratified turbulence [17,46,54] is immediately evident. Pairings between pancakes of like-signed vorticity gradually take place as the eddies grow in size but diminish in population. At higher Re, a slight distortion in pancake geometry is observed, although the ''pancakes'' exhibit a larger aspect ratio [17]. $Fr = \infty$ isosurfaces of vorticity magnitude (Fig. 5) exhibit much less organized structure of a smaller characteristic lengthscale. The vorticity field is organized in randomly oriented vortex tubes. Thinner and shorter tubes characterize the $Re = 2 \times 10^4$ unstratified visualizations as an increasingly finer structure is visible [13]. As expected in an unstratified turbulent flow, the features of coherent structures in the vorticity field are highly dependent on the vorticity magnitude threshold [32]. $Fr = \infty$ visualizations at even lower $|\omega|$thresholds do display quite a disorganized vorticity field but also events comparable to vortex rings as shown in Gourlay et al. [24].

A $y - z$ section of the horizontal velocity divergence

$$\Delta_z \equiv \frac{\partial u}{\partial x} + \frac{\partial v}{\partial y} \tag{46}$$

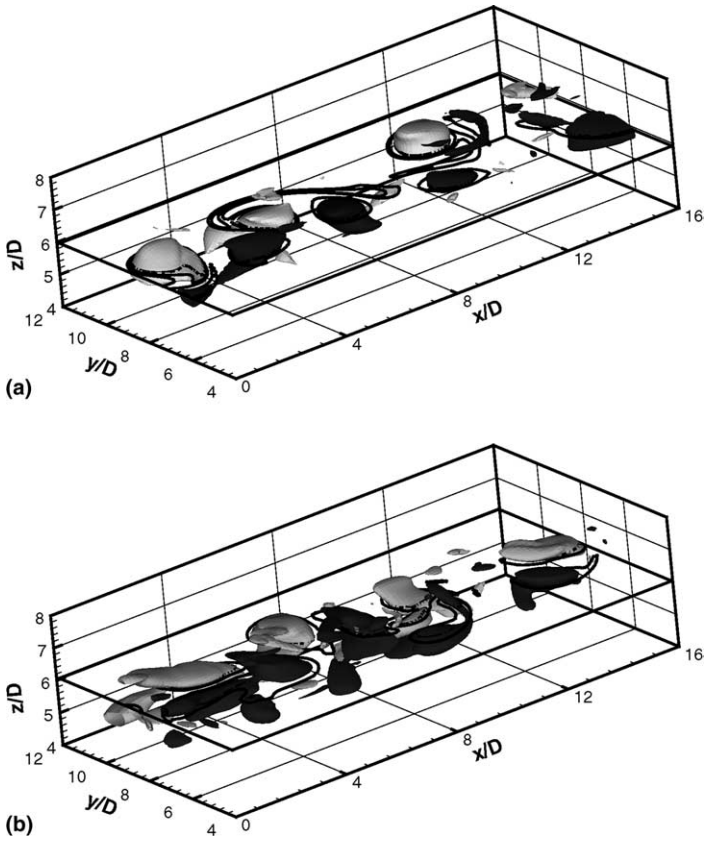

Fig. 4. Isosurfaces of vertical vorticity, ω_z in a y and z-truncated domain for the $Fr = 4$ simulations. Also shown are contours of ω_z at horizontal centerplane ($z = L_z/2$): (a) $Re = 5 \times 10^3$; (b) $Re = 2 \times 10^4$. Isosurface values are $1/2|\omega_z|_{\max}$ and $-1/2|\omega_z|_{\max}$ (light and dark color, respectively). Minimum/maximum contour values on centerplane slice are taken as half the minimum/maximum ω_z value in the flow.

is shown in Fig. 6 . At late times and the limit of low Froude number, Δ_z represents internal wave motions in the flow. At earlier times in the development of the stratified wake, where separation of internal waves and turbulence is not possible, Δ_z is simply an approximate and not exact descriptor of internal wave activity [54]. The radiation of internal waves from the stratified wake at relatively early times ($Nt = 15$) is evident in Fig. 6. Although the structure of Δ_z in the core of the wake is rather incoherent, emitted internal wave rays are seen propagating away at an angle of $\approx 45°$ from the vertical, as in the laboratory data [53]. Note that these propagating waves experience no reflections at the subdomain interfaces.

4.6. Model validation: quantitative results

A quantitative validation of the spectral multidomain model is provided by comparing results for mean flow quantities, the characteristic velocity and lengthscales in (43), with experimental data obtained over a range of Re and Fr. The values of U_0, L_Y and L_Z are obtained by performing a Gaussian fit according to (43) on the x-averaged mean profile calculated at individual sampling times in the run evolution. The model results are also compared to DNS results of Gourlay et al. [24] at $Re = 10^4$, $Fr = 10$ and LES data of Dommermuth et al. [13] at $Re = 10^4$, $Fr = 4$ mixed model LES (their corresponding $Re = 10^5$ results are not

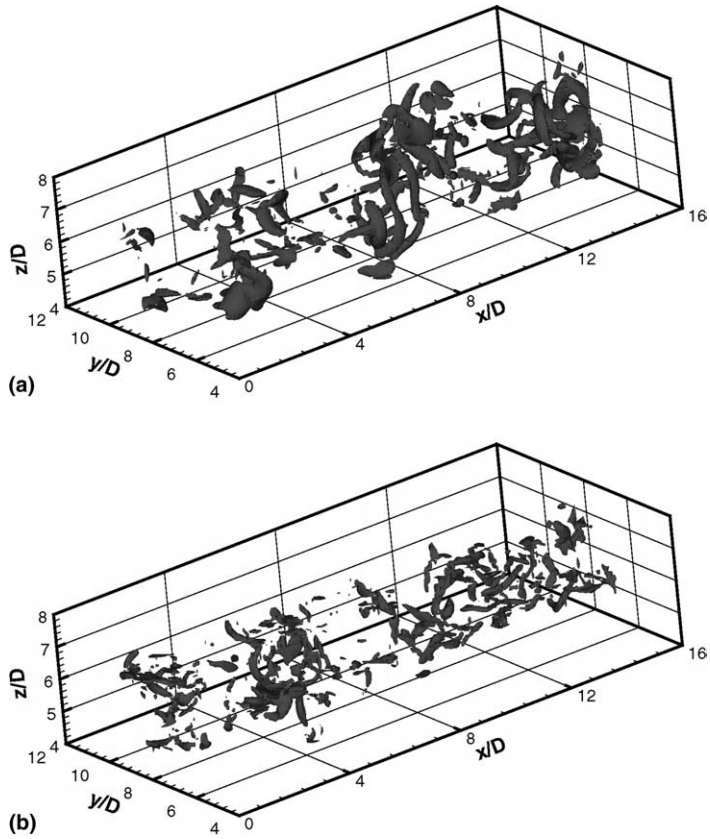

Fig. 5. Isosurfaces of vorticity magnitude $|\omega|$ in a y and z-truncated domain for the $Fr = \infty$ simulations: (a) $Re = 5 \times 10^3$; (b) $Re = 2 \times 10^4$. Isosurface value is $1/3|\omega|_{\max}$.

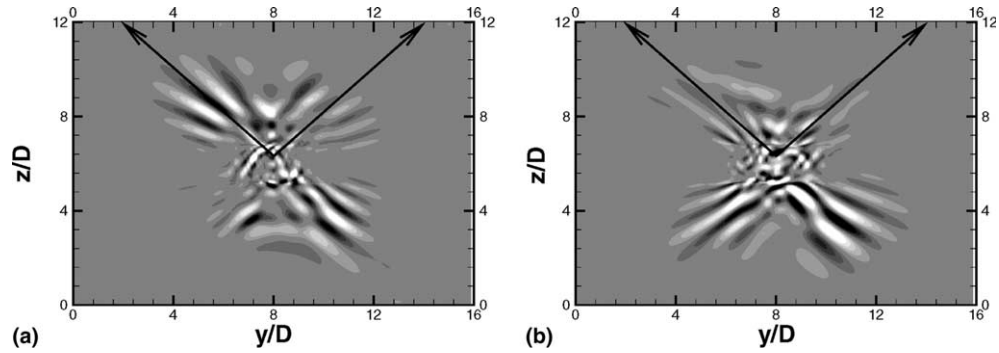

Fig. 6. Contours of horizontal velocity divergence, Δ_z at the vertical centerplane of the flow ($x = 0.5L_x$), for $Fr = 4$ sampled at time $Nt = 15$: (a) $Re = 5 \times 10^3$; (b) $Re = 2 \times 10^4$. Minimum/maximum contour values are taken as half the minimum/maximum value of Δ_z in the flow. The arrows indicate direction of internal wave propagation inclined at 45° with respect to the vertical.

different). Comparison with results from the laboratory and other numerical simulations is focused on the stratified case. The unstratified runs are not initialized with conditions equivalent to $Fr = \infty$ laboratory wakes at $x/D = 6$. Therefore, validation of the unstratified results is deemed sufficient if the timeseries conform to power laws derived from similarity analysis [56].

Note that this section presents only results pertaining to the larger resolved scales of the flow, as these scales are the ones least affected by spectral filtering. The filter affects these scales only indirectly, i.e., through non-linear interactions with the filtered scales. Thus, a stable and spectrally accurate numerical scheme, is anticipated to produce reliable results at the larger resolved scales [44,49]. Whether explicit spectral filtering may be viewed as a robust surrogate to conventional LES modelling would require detailed examination of quantities associated with the smallest-resolved scales, i.e., timeseries/profiles of turbulent kinetic energy and Reynolds stresses. Such an investigation lies outside the scope of this paper.

First, the maximum centerline velocity U_0 is considered in Fig. 7. Fig. 7 compares the spectral multidomain results with experimental data and other DNS/LES results. One of the distinguishing characteristics of stratified wakes is the presence of low mean kinetic energy decay rates in the non-equilibrium (NEQ) regime for $Nt \in [2,50]$ [51]. The SMPM simulations produce the same result. Both NEQ and quasi two-dimensional (Q2D) power law exponents for the decay of U_0 are within experimental uncertainty. The DNS and mixed model LES data exhibit similar behavior. No significant change is observed with increasing Re in the spectral multidomain data. The same plot (Fig. 7) also shows the evolution of the SMPM data for U_0 in the unstratified runs. For both values of Re, the unstratified wake does decay as a function of $x^{-2/3}$ determined by similarity analysis [56]. As also found in the laboratory [51,54], the stratified wake exhibits a higher value of U_0 and thus a higher mean energy density due to the constraining of the vertical wake scale L_Z by the stratification in the NEQ regime (see below).

The evolution of the wake horizontal lengthscale L_Y is shown in Fig. 8(a). Experimental observations show that the stratified wake grows in the horizontal at the exact same $x^{1/3}$ rate as its unstratified counter-

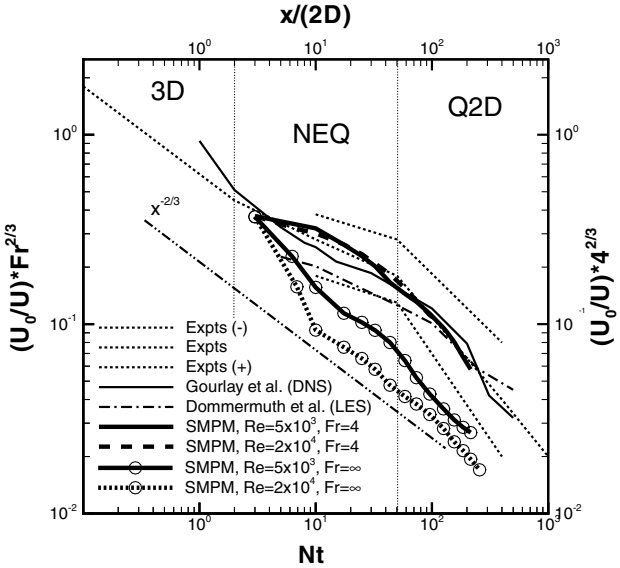

Fig. 7. Timeseries of the appropriate scaled maximum centerline mean velocity U_0. Comparison of $Fr = 4$ and ∞ SMPM results with data from experiments, DNS and mixed model LES. The Nt and $(U/U_0) \cdot Fr^{2/3}$ scaling for the abscissa and ordinate, respectively, is valid for all the stratified data. The $x/(2D)$ and $(U/U_0) \cdot Fr^{4/3}$ scaling is valid for comparing $Fr = 4$ to $Fr = \infty$ results. The dotted lines are the laboratory data of Spedding [51,54] where the middle line represents the mean value and the top/bottom lines correspond to the maximum deviation in the experimentally observed values. The vertical lines delineate the three distinct regimes of wake evolution [51]. Also shown is the $x^{-2/3}$ power-law predicted by self-similarity theory.

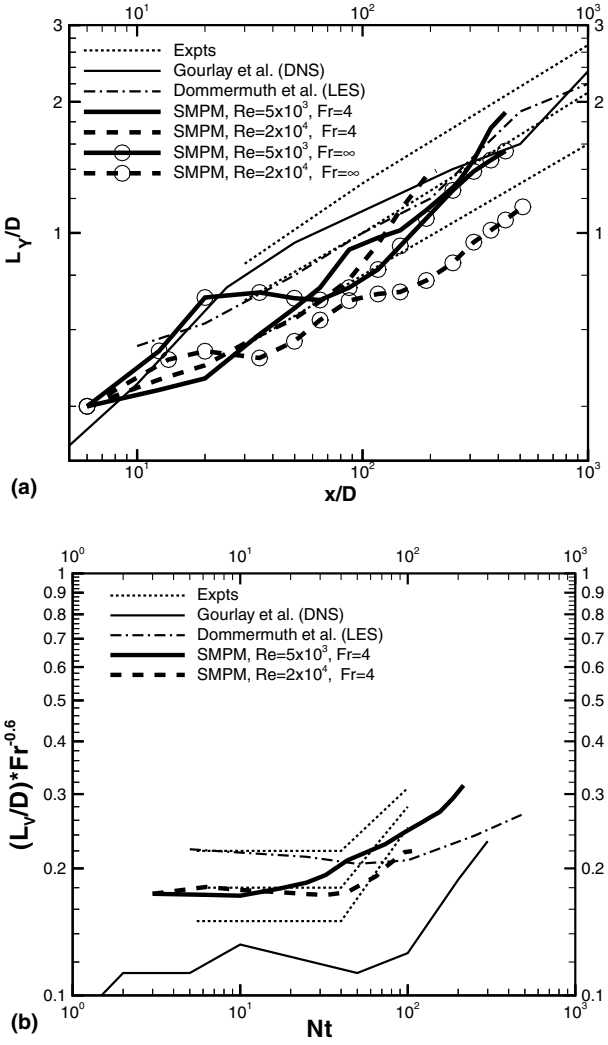

Fig. 8. Timeseries of appropriately scaled mean velocity profile lengthscales. The respective SMPM results are compared to the relevant Spedding laboratory data, DNS and mixed model LES. Dotted lines represent corresponding Spedding experimental data [51,53,54] as explained in Fig. 7. (a) SMPM results for horizontal wake lengthscale, L_Y at both $Fr = 4$ and ∞. The $Fr = 4$ Spedding experimental data evolves with the $x^{1/3}$ power law predicted by similarity theory. The horizontal variable is x/D. Lines with full triangles are normalized $Fr = \infty$ values of vertical lengthscale L_Z. (b) SMPM results for vertical wake lengthscale, L_Z at $Fr = 4$. The horizontal variable is Nt.

part [54,56]. Least-square fits to the SMPM data for both $Fr = 4$ cases indicate power law growth rates within the experimental uncertainty. The corresponding least square fits for the $Fr = \infty$ data show power law exponents very close to a value of 1/3. Throughout its entire evolution, the unstratified wake maintains comparable values of L_Y and L_Z (not shown) which is indicative of an axisymmetric growth, as one would expect [56].

Finally, timeseries of the wake vertical lengthscale L_Z for the $Fr = 4$ runs are shown in Fig. 8(b). Stratified wake experiments exhibit a phase of constant L_Z corresponding to the NEQ regime followed by a

transition to a $t^{0.6}$ growth rate in the Q2D regime [53]. Both trends are replicated by the SMPM data. The constant L_Z phase does end earlier in the $Re = 5 \times 10^3$ run. Nevertheless, both $Fr = 4$ simulations transition into a growth phase with power law exponents that appear to be closer to the experimental values than those of the mixed model LES data. The slight discrepancies in duration of the NEQ regime and the appearance of the breakpoint when the Q2D growth rate is established, should not be grounds for questioning the reliability of the spectral multidomain model. As discussed in detail by Spedding [51,53], both the duration of the NEQ regime and the transition into the Q2D phase appear to be dependent on the initial condition and specific forcing of the flow. Given that (see Section 4.2) the initial condition of a stratified wake simulation at $x/D = 6$ does not match exactly its experimental counterpart (asymmetry in mean/fluctuating profiles zero density perturbations, etc.) these weak discrepancies are justifiable.

5. Summary and concluding remarks

A spectral multidomain penalty method model has been developed for the solution of the three-dimensional incompressible Navier–Stokes equations under the Boussinesq approximation at high *Re*. A high accuracy splitting scheme is used based on a third order stiffly stable scheme for the non-linear term approximation, third order backward differentiation for the temporal derivatives and a high-order numerical boundary condition for the pressure. High spatial accuracy is established by Fourier spectral discretization in the periodic horizontal and variable height Legendre spectral multidomain discretization in the vertical, the latter allowing maximum flexibility in choice of boundary conditions and internal flow resolution. Simulations of high *Re* at resolutions of affordable cost are inherently under-resolved. To overcome problems of numerical stability due to under-resolution, moderate spectral filtering is applied in Fourier and Legendre space and the vertical discretization is supplemented with a multidomain penalty scheme and strong adaptive interfacial averaging. This is the first time a penalty method is applied to the simulation of a high *Re* incompressible flow, with a particular emphasis on the subdomain interfaces. The penalty method is applied separately at two levels in the numerical methodology: the non-linear term advancement and the viscous term treatment. Thus, examination of the internal high *Re* dynamics is possible without full resolution of the thin numerical/viscous physical boundary layers.

The laboratory flow chosen to validate the numerical model is a stratified turbulent wake with non-zero net momentum, with and without ambient stratification, at two different values of *Re*. The multidomain results capture correctly the various regimes of evolution and associated transition points observed in stratified laboratory wakes. The structure of the vorticity and internal wave fields of the stratified wake, at late and early-times, respectively, are also well reproduced by the model. The unstratified simulations exhibit power law exponents which agree with similarity theory while the associated vortical structure is comparable to that observed in previous DNS and LES. All results indicate that the model-resolved three-dimensional flow fields at the larger resolved scales, which are not directly influenced by the spectral filter, contain all the salient wake dynamics.

As claimed in certain recent studies, explicit filtering when combined with a higher order method, may serve as a viable alternative to conventional LES [44,49]. Such a claim may be justified by the common features such an approach shares with the alternative SGS modelling techniques (estimation model, spectrally vanishing viscosity, approximate deconvolution method) discussed in Section 1.3. However, as already indicated in Section 4.6, further work, focused on the computation of turbulent quantities (turbulent kinetic energy and dissipation rate, Reynolds stresses) is needed to affirm the reliability of high-order method and explicit filtering, when used in tandem, as a LES methodology. A future publication will focus on clarifying such a possibility. For now, the proposed model should simply be regarded as a filtered under-resolved DNS which attains (at considerably lower resolution) a *Re* twice as high as well-resolved DNS and provides reliable results at the large scales of the flow.

The spectral multidomain model appears well-suited for the investigation of localized stratified turbulent flows at higher *Re*. The resolution used, if compared to that required by DNS at similar *Re* [24], is a factor of four less in each direction, in particular at the early times of the simulation where the DNS cannot yet opt to regrid onto a large computational domain [24]. Therefore, high run repeatibility is possible. In regards to stratified turbulent wakes, the universality of scaling laws may be examined over a broad range of *Re* and *Fr*. The physical mechanisms behind the associated power law exponents may be elucidated by investigating the interaction between vortical and internal wave modes in the non-equilibrium (NEQ) regime and the late-time vertical growth of the wake. The flexibility in local flow resolution of the multidomain technique motivate application of the model to the study of the interaction of various localized stratified turbulent flows interacting with the vertical boundaries. Examples include the subsurface currents generated by internal wave radiation from the turbulent wake (a topic little explored in the existing literature [2]), a stratified turbulent patch [47] and resuspension effects occurring at the benthic boundary layer induced by travelling solitary internal waves [60]. Finally, the facility of implementation of complex boundary operators in the multidomain penalty scheme make it amenable to the study of geophysical flows with complex surface forcing (wind stress/buoyancy flux).

Acknowledgements

We thank Geoff Spedding for encouragement, physical insight and a thorough reading of an early draft of this paper. We also thank John Boyd, Frank Giraldo, Mohammed Iskandarani, George Karniadakis, Adam Fincham, Patrice Meunier, Jim Rottman, Kraig Winters and Frank Tse for useful discussion. We are grateful to an anonymous reviewer for extensive and constructive comments on an original version of this paper. P.J.D. is indebted to Professor John Diamessis, for unfaltering moral support and illuminating instruction on orthogonal polynomials. Jack Gibbons, John Burdette and Carl Gibson were instrumental in the funding of this project. This work was funded by ONR contract N00014-001-0756 administered by Dr. Ron Joslin. The work of the last author (J.S.H.) was partially supported by NSF through an NSF Career Award from the Division of Mathematical Sciences, and by the Alfred P. Sloan Foundation as a Sloan Research Fellow. Computation for the work described in this paper was supported by the University of Southern California Center for High Performance Computing and Communications (www.usc.edu/hpcc).

References

[1] H.M. Blackburn, S. Schmidt, Spectral element filtering techniques for large eddy simulation with dynamic estimation, J. Comput. Phys. 186 (2003) 610–629.
[2] V.G. Bondur, N.N. Filatov, Study of physical processes in the coastal zone for detecting anthropogenic impact by means of remote sensing, in: Proceedings of the 7th Workshop on Physical Processes in Natural Waters, Petrozavodsk, Russia, 2003, pp. 98–103.
[3] J.P. Boyd, Two comments on filtering (artificial viscosity) for Chebyshev and Legendre spectral and spectral element methods: preserving boundary conditions and interpretation of the filter as a diffusion, J. Comput. Phys. 143 (1998) 283–288.
[4] J.P. Boyd, Chebyshev and Fourier Spectral Methods, Dover, Mineola, New York, 2001.
[5] D.L. Boyer, D.B. Haidvogel, N. Perenne, Laboratory-numerical model comparisons of canyon flows: a parameter study, J. Phys. Oceanogr. 34 (7) (2004) 1588–1609.
[6] C. Canuto, M.Y. Hussaini, A. Quarteroni, T.A. Zang, Spectral Methods in Fluid Dynamics, Springer-Verlag, Berlin, 1988.
[7] A.B. Cortesi, G. Yadigaroglu, S. Banerjee, Numerical investigation of the entrainment and mixing processes in neutral and stably-stratified mixing layers, Phys. Fluids 11 (1999) 162–185.
[8] B. Costa, W.S. Don, On the computation of high order pseudospectral derivatives, Appl. Numer. Math. 33 (2000) 151–159.
[9] M.O. Deville, P.F. Fischer, E.H. Mund, High Order Methods for Incompressible Fluid Flow, Cambridge University Press, Cambridge, 2002.

[10] P.J. Diamessis, K.K. Nomura, The structure and dynamics of overturns in stably stratified homogeneous turbulence, J. Fluid Mech. 499 (2004) 197–229.
[11] J.A. Domaradzki, An analytic Green function's method in pseudo-spectral Navier–Stokes solvers for boundary layer and channel flows, J. Comput. Phys. 88 (1) (1990) 232–242.
[12] J.A. Domaradzki, K.C. Loh, P.P. Yee, Large eddy simulations using the subgrid scale estimation model and Truncated Navier–Stokes dynamics, Theor. Comput. Fluid Dyn. 15 (2002) 421–450.
[13] D.G. Dommermuth, J.W. Rottman, G.E. Innis, E.A. Novikov, Numerical simulation of the wake of a towed sphere in a weakly stratified fluid, J. Fluid Mech. 473 (2002) 83–101.
[14] W.S. Don, D. Gottlieb, J.H. Jung, A multidomain spectral method for supersonic reactive flows, J. Comput. Phys. 192 (2003) 325–354.
[15] W.S. Don, A. Solomonoff, Accuracy and speed in computing the Chebyshev collocation derivative, SIAM J. Sci. Comput. 16 (6) (1995) 1253–1268.
[16] D. Etling, Turbulence Collapse in Stably Stratified Flows: Application to the Atmosphere, Clarendon Press, Oxford, 1993 pp. 1–21.
[17] A. Fincham, T. Maxworthy, G. Spedding, Energy dissipation and vortex structure in freely decaying, stratified grid turbulence, Dyn. Atmos. Oceans 23 (1996) 155–169.
[18] P.F. Fischer, J.S. Mullen, Filtering techniques for complex geometry flows, Commun. Numer. Meth. Eng. 15 (1999) 9–18.
[19] D. Funaro, A multidomain spectral approximation of elliptic equations, Numer. Meth. Partial Diff. Equation 2 (1986) 187–205.
[20] D. Funaro, Domain decomposition methods for pseudo spectral approximations. Part I. Second order equations in one dimension, Numer. Math. 52 (1988) 329–344.
[21] R.P. Garg, J.H. Ferziger, S.G. Monismith, J.R. Koseff, Stably stratified turbulent channel flows. I. Stratification regimes and turbulence suppression mechanism, Phys. Fluids 12 (2000) 2569–2594.
[22] F.X. Giraldo, J.S. Hesthaven, T. Warburton, Nodal high-order discontinuous Galerkin methods for the spherical shallow water equations, J. Comput. Phys. 181 (2002) 499–525.
[23] D. Gottlieb, J.S. Hesthaven, Spectral methods for hyperbolic problems, J. Comput. Appl. Math. 128 (2001) 83–131.
[24] M.G. Gourlay, S.C. Arendt, D.C. Fritts, J. Werne, Numerical modeling of initially turbulent wakes with net momentum, Phys. Fluids 13 (2001) 3783–3802.
[25] J.L. Guermond, J. Shen, Velocity-correction projection methods for incompressible flows, SIAM J. Numer. Anal. 41 (1) (2003) 112–134.
[26] E. Hairer, S.P. Nørsett, G. Wanner, Solving Ordinary Differential Equations I. Non-stiff Problems, Springer Verlag, Berlin, 1987.
[27] H. Hanazaki, A numerical study of three-dimensional stratified flow past a sphere, J. Fluid Mech. 192 (1988) 393–419.
[28] J.S. Hesthaven, A stable penalty method for the compressible Navier–Stokes equations: II. One-dimensional domain decomposition schemes, SIAM J. Sci. Comput. 18 (3) (1997) 658–685.
[29] J.S. Hesthaven, A stable penalty method for the compressible Navier–Stokes equations: III. Multidimensional domain decomposition schemes, SIAM J. Sci. Comput. 20 (1) (1998) 62–93.
[30] J.S. Hesthaven, D. Gottlieb, A stable penalty method for the compressible Navier–Stokes equations: I. Open boundary conditions, SIAM J. Sci. Comput. 17 (3) (1996) 579–612.
[31] S.E. Holt, J.R. Koseff, J.H. Ferziger, A numerical study of the evolution and structure of homogeneous stably stratified sheared turbulence, J. Fluid Mech. 237 (1992) 499–539.
[32] K. Horiuti, A classification method for vortex sheet and tube structures in turbulent flows, Phys. Fluids 13 (12) (2001) 3756–3774.
[33] J. Imberger, Transport processes in lakes: review, in: R. Margalef (Ed.), Limnology Now: A Paradigm of Planetary Problems, North Holland/Elsevier Science Publishers B.V., Amsterdam, 1994, pp. 99–193.
[34] M. Iskandarani, D.B. Haidvogel, J.P. Boyd, A staggered spectral element model with application to the oceanic shallow water equations, Int. J. Numer. Meth. Fluids 20 (1995) 393–414.
[35] M. Iskandarani, D.B. Haidvogel, J.C. Levin, A three-dimensional spectral element model for the solution of the hydrostatic primitive equations, J. Comput. Phys. 186 (2003) 397–442.
[36] F.G. Jacobitz, S. Sarkar, C.W. Van Atta, Direct numerical simulations of the turbulence evolution in a uniformly sheared and stably stratified flow, J. Fluid Mech. 342 (1997) 231–261.
[37] L.H. Kantha, C.A. Clayson, Small Scale Processes in Geophysical Fluid Dynamics, Academic Press, San Diego, 2000.
[38] G.-S. Karamanos, G.E. Karniadakis, A spectral vanishing viscosity method for large-eddy simulations, J. Comput. Phys. 163 (2000) 22–50.
[39] G.E. Karniadakis, M. Israeli, S.A. Orszag, High-order splitting methods for the incompressible Navier–Stokes equations, J. Comput. Phys. 97 (1991) 414–443.
[40] R.M. Kirby, G.E. Karniadakis, Coarse resolution turbulence simulation with spectral vanishing viscosity-large eddy simulations (SVV-LES), J. Fluids Eng. 124 (2002) 886–891.
[41] P.K. Kundu, Fluid Mechanics, Academic Press, San Diego, 2002.

[42] J.G. Levin, M. Iskandarani, D.B. Haidvogel, A spectral filtering procedure for eddy-resolving simulations with a spectral element ocean model, J. Comput. Phys. 137 (1997) 130–154.
[43] J.T. Lin, Y.H. Pao, Wakes in stratified fluids, Ann. Rev. Fluid Mech. 11 (1979) 317–338.
[44] T.S. Lund, The use of explicit filters in large eddy simulation, Comp. Math. Appl. 46 (2003) 603–616.
[45] J.S. Mullen, P.F. Fischer, Filter-based stabilization of spectral element methods, CR Acad. Sci. Paris Serie I – Analyse Numerique 332 (1997) 265–270.
[46] J.J. Riley, M.P. Lelong, Fluid motion in the presence of strong stratification, Annu. Rev. Fluid Mech. 32 (2000) 613–657.
[47] J.J. Riley, R.W. Metcalfe, Direct numerical simulations of turbulent patches in stably-stratified fluids, in: Stratified Flows I, Proceedings of the 3rd International Symposium on Stratified Flows, California Institute of Technology, Pasadena, 1987.
[48] P. Sagaut, Large Eddy Simulation for Incompressible Flows: An Introduction, Springer Verlag, Berlin, New York, 2002.
[49] D.N. Slinn, J.J. Riley, A model for the simulation of turbulent boundary layers in an incompressible stratified flow, J. Comput. Phys. 144 (1998) 550–602.
[50] W.D. Smyth, K.B. Winters, Turbulence and mixing in Holmboe waves, J. Phys. Oceanogr. 33 (4) (2003) 694–711.
[51] G.R. Spedding, The evolution of initially turbulent bluff-body wakes at high internal Froude number, J. Fluid Mech. 337 (1997) 283–301.
[52] G.R. Spedding, Anisotropy in turbulence profiles of stratified wakes, Phys. Fluids 13 (8) (2001) 2361–2372.
[53] G.R. Spedding, Vertical structure in stratified wakes with high initial Froude number, J. Fluid Mech. 454 (2002) 71–112.
[54] G.R. Spedding, F.K. Browand, A.M. Fincham, Turbulence, similarity scaling and vortex geometry in the wake of a towed sphere in a stably stratified fluid, J. Fluid Mech. 314 (1996) 53–103.
[55] S. Stolz, N.A. Adams, An approximate deconvolution procedure for large-eddy simulation, Phys. Fluids 11 (1999) 1699–1701.
[56] H. Tennekes, J.L. Lumley, A First Course in Turbulence, The MIT Press, Cambridge, 1972.
[57] S.A. Thorpe, Turbulence in the stratified and rotating world ocean, Theor. Comput. Fluid Dyn. 11 (1998) 171–181.
[58] J. Trujillo, G.E. Karniadakis, A penalty method for the vorticity–velocity formulation, J. Comput. Phys. 149 (1999) 32–58.
[59] K.L. Tse, A. Mahalov, B. Nicolaenko, H.J.S. Fernando, Quasi-equilibrium dynamics of shear-stratified turbulence in a model tropospheric jet, J. Fluid Mech. 496 (2003) 73–103.
[60] B.J. Wang, L.G. Redekopp, Long internal waves in shear flows: topographic resonance and wave-induced global instability, Dyn. Atmos. Oceans 33 (2001) 263–302.
[61] K.B. Winters, J. McKinnon, B. Mills, A spectral model for process studies of density stratified flows, J. Atmos. Ocean. Techn. 21 (1) (2004) 69–94.
[62] C. Xu, R. Pasquetti, Stabilized spectral element computations of high Reynolds number incompressible flows, J. Comput. Phys. 196 (2004) 680–704.